

Discovery of the HCV NS3/4A Protease Inhibitor (1R,5S)-N-[3-Amino-1-(cyclobutylmethyl)-2,3-dioxopropyl]-3-[2(S)-[[[(1,1-dimethylethyl)amino]carbonyl]amino]-3,3-dimethyl-1-oxobutyl]-6,6-dimethyl-3-azabicyclo[3.1.0]hexan-2(S)-carboxamide (Sch 503034) II. Key Steps in Structure-Based Optimization

Andrew J. Prongay,* Zhuyan Guo, Nanhua Yao, John Pichardo, Thierry Fischmann, Corey Strickland, Joseph Myers, Jr., Patricia C. Weber, Brian M. Beyer, Richard Ingram, Zhi Hong, Winifred W. Prossise, Lata Ramanathan, S. Shane Taremi, Taisa Yarosh-Tomaine, Rumin Zhang, Mary Senior, Rong-Sheng Yang, Bruce Malcolm, Ashok Arasappan, Frank Bennett, Stephane L. Bogen, Kevin Chen, Edwin Jao, Yi-Tsung Liu, Raymond G. Lovey, Anil K. Saksena, Srikanth Venkatraman, Viyyoor Girijavallabhan, F. George Njoroge, and Vincent Madison

Schering-Plough Research Institute, 2015 Galloping Hill Road, Kenilworth, New Jersey 07033

Received February 15, 2006

The structures of both the native holo-HCV NS3/4A protease domain and the protease domain with a serine 139 to alanine (S139A) mutation were solved to high resolution. Subsequently, structures were determined for a series of ketoamide inhibitors in complex with the protease. The changes in the inhibitor potency were correlated with changes in the buried surface area upon binding the inhibitor to the active site. The largest contribution to the binding energy arises from the hydrophobic interactions of the P1 and P2 groups as they bind to the S1 and S2 pockets [the numbering of the subsites is as defined in Berger, A.; Schechter, I. *Philos. Trans. R. Soc. London, Ser. B* **1970**, 257, 249–264]. This correlation of the changes in potency with increased buried surface area contributed directly to the design of a potent tripeptide inhibitor of the HCV NS3/4A protease that is currently in clinical trials.

Introduction

Approximately 170 million people worldwide are infected with the hepatitis C virus (HCV), the etiologic agent of non-A non-B hepatitis.¹ Current combination therapy of pegylated-interferon- α and ribavirin gives 70–80% sustained virological response against most genotypes, but only 40% against genotype 1.² Consequently, the discovery of more effective anti-HCV agents has been a major objective of pharmaceutical companies. Extensive biochemical and structural studies have been performed on the NS3/NS4A serine protease and the NS5B RNA polymerase. Significant progress has been made in the structure-based design (SBD) of inhibitors of these enzymes as summarized in a review.³ Herein, we will focus on the SBD of inhibitors of the HCV NS3/NS4A protease and refer to it simply as the HCV protease.

There have been several studies of the three-dimensional structure of HCV protease, including the holo-enzyme and inhibitor complexes. There are now several released crystal structures of the HCV protease in the PDB from genotype 1 utilizing one of three strains, BK(1b), H(1a), and J(1b) strains. The first crystal structure (H strain) revealed that the protease has a chymotrypsin-like fold, a classical Asp-His-Ser catalytic triad, and the NS4A cofactor intercalated within a β -sheet of the enzyme core [1A1R].⁴ A simultaneous publication of just NS3 without the NS4A cofactor (BK strain) showed the same core structure, but with unfolding of residues 1–30 at the N-terminus and an altered conformation of residues 60–72 in the β -hairpin near the NS4A intercalation site [1A1Q].⁵ Subsequent NMR studies of the solution structure of NS3 protease domain also showed disorder of residues 1–21 and altered β -hairpin conformations [1BT7, 1DXW].⁶

The NS3 sequences in these three strains are highly homologous (89–97% pairwise identity), and the protease structures are very similar for the holoprotein and inhibitor complexes. Using the original H strain structure as a reference [1A1R], the seven other H [1N1L, 1RGQ, 1RTL] and J [1DXP, 1DY8, 1DY9, 1W3C] strain structures fit within average RMSDs of 0.43 Å for the C α s and 1.03 Å for all atoms spanning the common residues 3–175. The BK strain structures [1CU1, 1JXP, 1NS3] have somewhat larger differences from the reference structure with average RMSDs of 0.83 Å for C α s and 1.34 Å for all atoms.

The binding modes of inhibitors have been elucidated in multiple structures of inhibitor/protease complexes. The bifunctional protease–helicase is auto-inhibited by binding the six C-terminal residues of the helicase domain as the P-side product of the *cis* cleavage of the NS3–NS4A junction [1CU1].⁷ The product peptide binds in an antiparallel direction with five backbone hydrogen bonds from the P5, P3, and P1 residues to the edge β -strand of the protease domain and also H-bonds from the terminal carboxylate to the catalytic His57 and the oxyanion hole. The S5 pocket is formed by three residues from the helicase domain. Apparently the interactions between the helicase and the protease domains are easily disrupted because both the catalytic efficiency and the inhibitor binding strength are comparable for the full-length NS3/NS4A and the truncated form missing the helicase domain.⁸ None of the other structures include the NS3 helicase domain.

For product-based hexapeptide inhibitors, it has been shown that optimization of the P6–P1 residues substantially increases potency.⁹ Structures of the complexes from NMR and modeling studies¹⁰ as well as in-house crystallographic studies exhibit the same binding features as the product peptide in the bifunctional enzyme. A potent, macrocyclic tetrapeptide product inhibitor

* To whom correspondence should be addressed. Tel.: (908) 740-3406. Fax: (908) 740-4844. E-mail: andrew.prongay@spcorp.com.

has also been discovered that advanced to proof-of-concept clinical trials.^{11,12} NMR and crystallographic studies showed that a close analog of this inhibitor has the same binding mode with additional interactions from a unique, large P2 group.^{13,14}

Other published structures of inhibitor/protease complexes feature a covalent bond linking the catalytic Ser139 to one of four types of electrophile in the inhibitor. First, three ketoacid complexes of the general type Cap-P3-Leu-F₂Abu-CO-COOH [1DY8, 1DY9, 1W3C] (F₂Abu = 2-amino-4,4-difluoro-butyric acid) share many features with the product inhibitor complexes. New features of these inhibitors arise from *si*-face attack on the keto group by Ser139 to form a tetrahedral adduct. The oxygen from the keto group H-bonds to His57, and both carboxylate oxygens form H-bonds to NHs in the oxyanion hole. The Cap group partially occupies the S4 subsite. Second, the structure of the protease complexed to a ketoamide inhibitor of the type Cap-P4-P3-P2-P1-CO-P1' [1RGQ] shares the backbone H-bonds and tetrahedral adduct geometry of the ketoacids. In this case, the CO of the P1-P1' peptide bond forms two H-bonds with NHs of the oxyanion hole. The CO group of the Cap mimics a backbone H-bond of the product inhibitor P5 residue. Brief descriptions have been published of the ketoamide and side-chain interactions in additional crystal structures of ketoamide inhibitors complexed with the protease.^{15–21} Two inhibitors from this class are currently in clinical trials.^{22,23} A third inhibitor type features formation of an acyl enzyme adduct following attack by Ser139 to open a lactam ring [1NIL, 1RTL]. The lactam CO forms H-bonds in the oxyanion hole, and the amide NH of the lactam H-bonds to His57. Fourth, a brief communication has reported the structure of a similar acyl enzyme from attack of an inhibitor aldehyde group.²⁴

Herein we report the solution of the holo-HCV protease crystal structure to high resolution using the inactive S139A mutant. Optimization of ketoamide inhibitors will be traced and correlated with the structures of the inhibitors and their complementarity to the enzyme binding site revealed in crystallographic structures of protease/inhibitor complexes. This process culminated in the discovery of the tripeptide ketoamide, (1*R*,5*S*)-*N*-[3-amino-1-(cyclobutylmethyl)-2,3-dioxopropyl]-3-[2(*S*)-[[[(1,1-dimethylethyl)amino]carbonyl]amino]-3,3-dimethyl-1-oxobutyl]-6,6-dimethyl-3-azabicyclo[3.1.0]hexan-2(*S*)-carboxamide, (SCH503034, hereafter referred to as Compound 19), which has advanced to clinical trials as a potential treatment for HCV infections.²⁵

Experimental Section

Cloning, Mutagenesis, and Protein Expression. The catalytic domain of NS3(1–181) was cloned from cDNA (obtained from Dr. Charles Rice, Washington University at St. Louis) isolated from the H77 strain of HCV genotype 1a. The NS3 domain was fused with a T7 tag (MASMTGGQMG) at the N-terminus and with a His tag (GSHHHHHH) at the C-terminus to generate the protease construct described by Kim et al.⁴ A mutant NS3 (T7 and His-tagged) protease (Ser139 to Ala139 mutation) was created using site-directed mutagenesis by the polymerase chain reaction. Both the native and S139A mutant (T7 and His-tagged) NS3 constructs were subcloned into the pET-3a (Novagen) vector, and the resulting expression plasmids were then co-transformed with the pREP4 (Novagen) plasmid into the bacterial host, BLR21(DE3). Freshly transformed *E. coli* BLR21(DE3) cells were grown in LYM-1 media containing 50 μ g/mL kanamycin and 100 μ g/mL ampicillin.

Large-Scale Cell Growth and Protein Purification. *E. coli* cell growth and protein purification were performed as previously described⁴ with a few modifications for large scale (100 L) prepara-

tions. The S139A mutant was expressed and purified using procedures analogous to those for the T7/His-tagged “native” construct.

Crystallization. The NS3 protease domain was complexed with the NS4A peptide (KKGSVVIVGRIVLSGKPAIIPKK) at a 1:2 molar ratio and crystallized using a modification of a previously published protocol.⁴ The complex was passed through a Pharmacia Sephacryl S-100 HR16/60 resin equilibrated with 15 mM MES, pH 6.5, 1.0 M NaCl, 1% (w/v) glycerol, and 10 mM β -mercaptoethanol. The pooled fractions containing the complex were concentrated to 10–15 mg/mL using a Millipore Ultrafree Biomax-5K centrifugal filtration device. Prior to setting up crystallization trials, the protein solution was centrifuged at 300 000 \times g for 1 h at 4 °C. Crystallization was performed by the vapor diffusion method using hanging drops (4 μ L protein solution mixed with 4 μ L of 0.75–1.00 M NaCl, 0.1 M MES, 0.1 M Na/KPO₄, pH 5.6–6.2) suspended over 1 mL reservoir solutions of 1.25–1.50 M NaCl, 0.1 M MES, 0.1 M Na/KPO₄, 5 mM β -mercaptoethanol, pH 5.6–6.2. All chemical reagents were of the highest quality available. The trays were incubated at 4 °C for 5–7 days to control nucleation, followed by incubation for 3 weeks at 12 °C to maximize crystal growth. Crystals grew as large as 250 μ m \times 250 μ m \times 600 μ m. The S139A mutant NS3/NS4A peptide complex crystallized under conditions analogous to those for the “native” construct and grew as large as 300 μ m \times 300 μ m \times 500 μ m.

Preparation of Heavy Atom Derivatives. Heavy atom derivatives of crystalline T7/His-tagged NS3/NS4A peptide complex, grown at pH 6.2, were prepared by soaking in 1 mM K₂PtCl₄ in 1.7 M NaCl, 0.11 M Na/KPO₄, 0.11 M MES, pH 6.2, overnight at room temperature, soaking in 0.1 mM HgCl₂ for 1 h, or soaking for 1 h in a 1:10 dilution of a saturated solution of chloromercurifuran in the same buffer. All of the heavy atom compounds were prepared in 1.7 M NaCl, 0.11 M Na/KPO₄, 0.11 M MES, pH 6.2. The soaked crystals were transferred to a cryo-protectant solution (1.7 M NaCl, 0.11 M Na/KPO₄, 0.11 M MES, pH 6.2, 25% glycerol), frozen in liquid propane, and stored in a Dewar filled with liquid nitrogen.

Preparation of Inhibitor Complexes of HCV Protease. All of the inhibitors for which structures were determined were dissolved in 100% DMSO to 1–5 mM final concentrations. These solutions were diluted 1:100 with 1.6 M NaCl, 0.11 M MES, 0.11 M Na/KPO₄, pH 5.7, 10 mM β -mercaptoethanol. Crystals of native enzyme were transferred into 300 μ L of the buffered inhibitor solutions and soaked overnight at room temperature. The crystals were then transferred to 300 μ L of 1.6 M NaCl, 0.11 M MES, 0.11 M Na/KPO₄, pH 5.7, 10 mM β -mercaptoethanol, 42% (w/v) sucrose, prior to freezing in liquid propane.

X-ray Data Collection and Processing. X-ray diffraction intensities were collected using various detectors and X-ray sources. The “home sources” have included a Rigaku R-Axis IIC image plate detector mounted on a Rigaku RU200 rotating anode generator at 100 mA and 50kV; a Rigaku R-Axis IV image plate detector mounted on a Rigaku RU-H3R generator; and a Rigaku R-Axis HTC image plate detector mounted on a Rigaku FR-E generator. Data were also collected at the Cornell High Energy Synchrotron Source A-1 beamline and at the IMCA-CAT beamlines 17ID and 17BM at the Advanced Photon Source at the Argonne National Laboratories. The 17ID beamline has employed both a Bruker CCD and ADSC Q-210 CCD detectors, while a Mar345 and a MarCCD have been in use at the 17BM beamline. Data were collected to 2.5 Å for the native crystal, 3.5 Å for both the mercury and platinate derivative crystals, and 2.0 Å for the S139A crystal. Datasets of crystals soaked with inhibitors were collected to resolutions ranging from 3.2 to 2.0 Å. Intensities were integrated and scaled using the HKL and Scalepack programs.²⁶

Structure Solution and Refinement. The crystal structure of the native HCV protease was determined by multiple isomorphous replacement (MIR) using the mercury and platinate heavy atom derivatives. Two major heavy atom sites in the mercury map were located by inspection of the Harker sections of difference Patterson maps, which were calculated using a weakly derivatized crystal as

Table 1. Data Collection and Refinement Statistics

data set	native	S139A mutant	compound 1	compound 15	compound 19	compound 22	compound 36
unit cell	$a = b =$ 225.57 Å $c = 75.72$ Å	$a = b =$ 224.39 Å $c = 75.33$ Å	$a = b =$ 222.94 Å $c = 75.16$ Å	$a = b =$ 224.26 Å $c = 75.45$ Å	$a = b =$ 223.87 Å $c = 74.96$ Å	$a = b =$ 224.27 Å $c = 75.21$ Å	$a = b =$ 224.68 Å $c = 75.60$ Å
limiting resolution (Å)	2.5	2.0	2.7	2.25	2.65	2.6	2.7
unique reflections	22 724	46 263	19 638	33 806	20 317	22 055	18 800
avg multiplicity	1.9	2.7	3.6	4.2	5.3	2.2	3.6
completeness ^a (%)	89.4 (76.3)	94.9 (65.6)	99.7 (99.8)	98.7 (83.1)	97.1 (70.0)	99.0 (99.3)	93.8 (56.4)
R_{sym} ^b (%)	6.6 (27.6)	4.4 (46.4)	5.0 (41.3)	4.7 (41.1)	4.1 (25.7)	6.9 (46.6)	4.3 (26.7)
$I/\sigma I$	11.7 (2.3)	18.6 (1.4)	23.3 (3.3)	26.4 (2.3)	31.6 (3.5)	11.4 (2.2)	23.8 (2.2)
Refinement Statistics							
resolution range (Å)	8.0–2.5	12.0–2.0	8.0–2.7	8.0–2.3	8.0–2.66	8.0–2.6	8.0–2.7
nonhydrogen atoms	2896	2989	2984	2940	2987	2958	3040
R_{work} (%)	26.4	26.0	20.4	19.5	18.1	17.6	18.8
R_{free} ^c (%)	20.3	21.9	25.9	25.8	27.6	28.8	29.3
r.m.s. bond length (Å)	0.008	0.008	0.009	0.009	0.009	0.008	0.008
r.m.s. bond angle (°)	1.9	1.86	1.94	1.98	1.91	1.82	1.84
average B (Å ²)	25.1	24.7	31.8	33.4	39.5	28	35.3
Number of Residues in the Different Regions of the Ramachandran Plot							
nonallowed	0 (0.0%)	0 (0.0%)	0 (0.0%)	0 (0.0%)	0 (0.0%)	0 (0.0%)	0 (0.0%)
generously allowed	0 (0.0%)	0 (0.0%)	0 (0.0%)	0 (0.0%)	2 (0.3%)	0 (0.0%)	0 (0.0%)
additional allowed	63 (11.5%)	55 (8.8%)	58 (10.0%)	43 (6.7%)	64 (10.7%)	67 (12.3%)	53 (9.7%)
most favored	481 (88.5%)	574 (91.2%)	523 (90.0%)	603 (93.3%)	530 (89%)	480 (87.7%)	492 (90.3%)
PDB ID number	2OBQ	2O8M	2OC1	2OC0	2OC8	2OBO	2OC7

^a Values reported are overall and the values in parentheses are for the highest resolution shell. ^b R_{sym} is defined as $\sum |I - \langle I \rangle| / \sum I$, where I = observed intensity, $\langle I \rangle$ = average over Friedel and symmetry equivalents. ^c R_{free} was calculated with 4% of the data. All reflections within the specified resolution ranges were used in the refinement.

the native dataset. Minor mercury and platinum sites were located by difference Fourier methods. Heavy atom phasing, combined with solvent flattening, resulted in an interpretable 3.2 Å electron density map in which the domains of the two β-barrel regions of the structure were clearly defined. Local symmetry restraints were not applied during refinement. At a resolution of 2.5 Å, water molecules were added. R_{free} was closely monitored throughout the entire structure determination. The structure of the S139A mutant was determined to be 2.0 Å, with the native structure as a phasing model using the Xplor program.²⁷ The structures of the ketoamide inhibitor–protease complexes were determined by difference Fourier methods using the coordinates of the S139A structure to generate the calculated amplitudes and phases. This is the sole use of the S139A mutant structure for the discussions herein.

Accessible Surface Area and Energy Calculations. The binding free energy due to the hydrophobic effect is proportional to the buried surface area.²⁸ The buried surface area was calculated from the crystal structures of protease/inhibitor complexes using the Sybyl program package²⁹ and the Connolly molecular surface program.³⁰ Hydrogen atoms were added to the inhibitor and the protease using standard covalent geometry. Exposed surface areas in the complex were calculated separately for the P side chain and the S site. For the uncomplexed state, free surface areas were calculated for the P side chain and for the S site with the inhibitor removed from the protease complex. The buried surface area is the difference between that of the uncomplexed state and that of the complexed state. The total buried surface area (ΔSA) is the sum of that from the P side chain and the S sites. For inhibitor i relative to a reference inhibitor $\Delta \Delta SA = \Delta SA_i - \Delta SA_{\text{ref}}$ and the increase in binding affinity due to the hydrophobic effect is $10^{(\Delta \Delta SA/30 \text{ \AA}^2)}$.²⁸

Synthesis and Assay of Inhibitors. Chemical synthesis, purification, and characterization of the inhibitors are described in another paper.²³ The ketoamide inhibitors have reversible tight binding kinetics. A continuous assay³¹ was used to determine K_i^* values.³²

Results

NS3/NS4A Structure. For this study, the HCV protease with the sequence from the genotype H 1a strain was utilized with the chain termini, as defined in the Experimental Section.

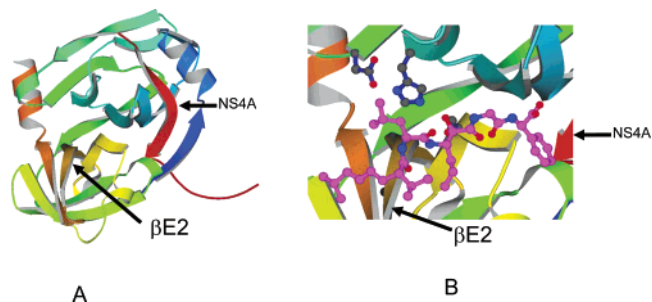


Figure 1. Ribbon drawing of HCV NS3/4A protease domain. (A) The tertiary structure of a monomer of the protease domain is presented as a ribbon drawing. The ribbon progresses through a rainbow coloring starting with a blue N terminus and ending with an orange C-terminus. The NS4A peptide is shown in red. (B) The view is zoomed on the active site. The side chains of the active site triad are shown as ball-and-stick models with dark blue sticks and a standard atom specific coloring for the balls. Inhibitor 1 is represented as a ball-and-stick model, with the carbon atoms and all the bonds pink, nitrogens are dark blue, and oxygens are red. The orientation of the view of the protease is the same in both panels. These figures were generated using the program Molscript.³³

Crystallization, data collection, and refinement procedures are also described above. The crystallographic data for the holo native, the S139A mutant, and for the five protease–inhibitor complexes structures are presented in Table 1. The structure of the native protease was solved by MIR, using data from a crystal that had been weakly derivatized with a mercury compound as the reference and data from crystals with higher occupancy of mercury and platinum compounds to define the heavy atom positions. The native structure was used to solve the S139A mutant structure, which extends to higher resolution (2.0 Å). Without the catalytic serine, the S139A mutant of the HCV NS34A protease is inactive. The current structure of native HCV protease recapitulates the previously published features of this chymotrypsin-like serine protease and is nearly identical in detail. The protein crystallizes as a dimer in the asymmetric unit. Figure 1 is a ribbon representation of the monomeric

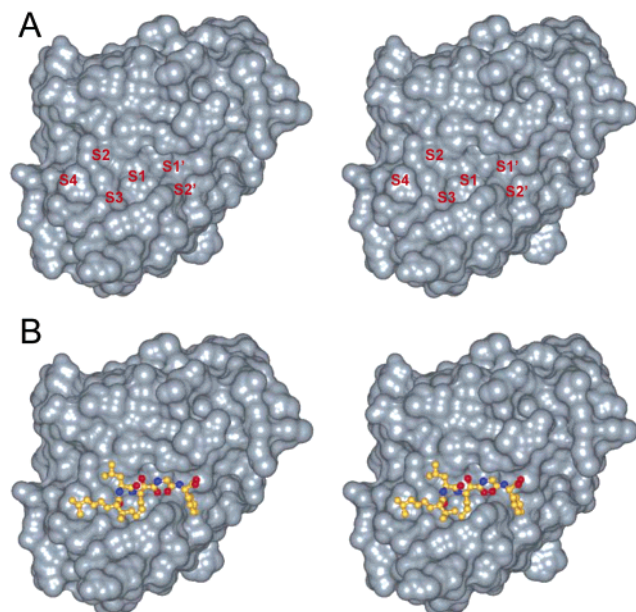


Figure 2. Connolly surface representations of the protease domain. A stereo presentation of the Connolly surface of a monomer of the HCV NS3/4A protease domain. The C-terminal nine residues on the NS4A peptide have been removed for clarity. The protein is a dimer in the crystal. Panel A: The surface of the protein from its complex with **1**. The S4–S2' binding pockets are labeled in red. Panel B: The bound inhibitor **1** is shown as a ball-and-stick model, with the carbons in orange, the nitrogens in blue, and the oxygens in red. These figures were generated using the program InsightII.³⁴

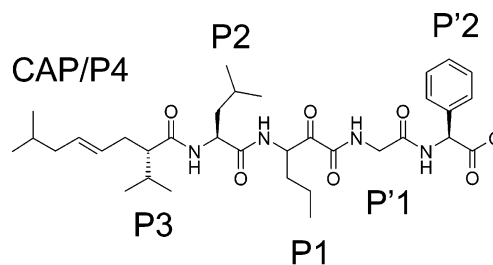
structure showing strand $\beta E2$ poised to accept hydrogen bonds from an antiparallel strand in substrates or inhibitors and the 4A peptide intercalated into the structure near the binding site. A close-up view of bound inhibitor **1** shows the Asp-His-Ser catalytic triad (Figure 1B). When the same reference structure as in the Introduction is used [1A1R], the current structure has RMSDs of 0.19 Å for C α s and 1.10 Å for all atoms. The native and mutant structures are essentially identical; RMSDs between the two current structures are 0.17 Å for C α s and 0.76 Å for all atoms. Because the structure of the S139A mutant is refined to higher resolution than the native structure, it was used as the starting point in solving structures of subsequent protease–inhibitor complexes by difference Fourier methods. However, because the ketoamide inhibitors form a reversible covalent bond with the active site serine139, their protease complexes were generated by soaking the inhibitors into crystals of the catalytically competent, native enzyme.

Substrate Binding Site. Figure 2A shows the protein surface with subsites labeled. The surface is rather flat with minor surface depressions. S1 is the largest and best defined cavity. Our discovery process from an initial ketoamide-containing undecapeptide lead through P3–P2' derived pentapeptide mimics and ultimately to the tripeptide P3–P1 mimic, **19**, is traced in another paper.²³ Herein, the structural path is traced beginning with Inhibitor 1, a pentapeptide ketoamide inhibitor. To illuminate this path, complete crystallographic data are given for five benchmark protease–inhibitor complexes (Table 1). In all cases, only one of the two protease molecules in the asymmetric unit is complexed with an inhibitor. The coordinates of these five structures and the two holo-enzyme structures have been deposited in the PDB. To buttress the analysis based on these key structures (Table 2), dozens of unpublished protease–inhibitor structures were also used. The chemical structures and

Table 2. Protease–Inhibitor Crystal Structures Presented Herein

Compound	Chemical Structure	HCV K_i^* nM
1		4300
15		15
19		14
22		57
36		1400

residue names for the entities used at inhibitor subsites are defined in Table 3.

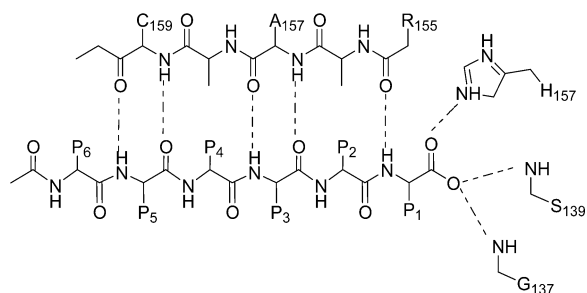


Inhibitor 1.

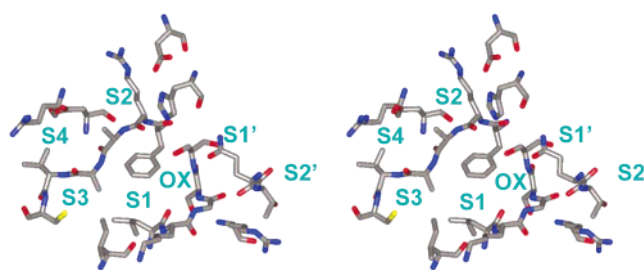
The structure derived from a crystal soaked with **1** shows a covalent complex with the inhibitor that spans subsites S4–S2'. The aliphatic cap of **1** is analogous to IBoc-Val as P4–P3. The *si*-face attack of Ser139 yields a stable tetrahedral intermediate with a covalent bond from Ser O γ to the keto carbon and with the keto oxyanion hydrogen bonded to His57. The P1 amide carbonyl oxygen is in the oxyanion hole H-bonding to the NHs of Gly137 and Ser139 (Figure 3). Canonical backbone H-bonds are formed: P3CO-Ala157NH, P1NH-Arg155CO, P2'NH-Thr42CO, and P2'CO-Thr42NH. P3 lacks an amide NH, so the usual P3NH-Ala157CO H-bond is missing. The inhibitor

Table 3. Residue Names and Chemical Structures

Residue	Name	Structure	Residue	Name	Structure
c-Bua	Cyclobutylalanine		Chg	Cyclohexylglycine	
c-Bua-F2	Difluorocyclobutylalanine		DCCP	Dichlorocyclopropylproline	
c-Bug	Cyclobutylglycine		DFCP	Difluorocyclopropylproline	
c-Pea	Cyclopentylalanine		DMCP	Dimethylcyclopropylproline	
c-Peg	Cyclopentylglycine		DMFP	Dimethylfuranlyproline	
c-Pra	Cyclopropylalanine		t-Bua	t-Butylalanine	
c-Pra-F2	Difluorocyclopropylalanine		t-Bug	t-Butylglycine	
c-Prg	Cyclopropylglycine		ODBP	1-oxo-2-dimethyl-cyclobutylproline	
Cha	Cyclohexylalanine				

**Figure 3.** Canonical backbone H-bonding interactions. The schematic drawing demonstrates the H-bonding interactions that form between the protease strand E2 and peptidic inhibitor molecules. The G137 and S139 backbone NHs forming the oxyanion hole are also shown.

side chains bind in surface pockets that are primarily hydrophobic, with the S1 pocket being the largest and deepest (Figure 2B). The residues that define each of the binding subsites are shown in Figure 4 and Table 4. The polar head groups of protein residues in the binding site interact with each other or with solvent. Compared to the structures of the holo-enzyme, there are only a few adjustments of side-chain conformations upon complexing **1**. Side chains that adjust include Arg123, Ile132, Lys136, Arg155, Cys159, and Asp168. Analysis of 21 additional protease-inhibitor complexes reveals that these are the only side chains that adjust from the holo-enzyme structures (Figure

**Figure 4.** Stereoview of the inhibitor binding site. Stereo of the inhibitor binding pocket in an atom-colored stick representation with sub-sites labeled (InsightII³⁴).**Table 4.** Side chains Forming Binding Subsites

S4	R123, A156, ^a V158, D168
S3	I132, ^a A157, ^a C159
S2	H57, D81, R155, A156 ^a
S1	I132, ^a L135, K136, ^a G137, ^a S138, ^a S139, ^a F154, A157
S1'	Q41, ^a G137, ^a S138, ^a S139 ^a
S2'	Q41, ^a T42, R109, K136 ^a

^a Part of two binding sites.

5A). Arg155 and Cys159 have a single conformation in all of the complexes (Table 5). Arg155 shifts from no intramolecular polar interactions to a position in which it forms a salt bridge with Asp81 of the catalytic triad. Cys159 shifts to enlarge the

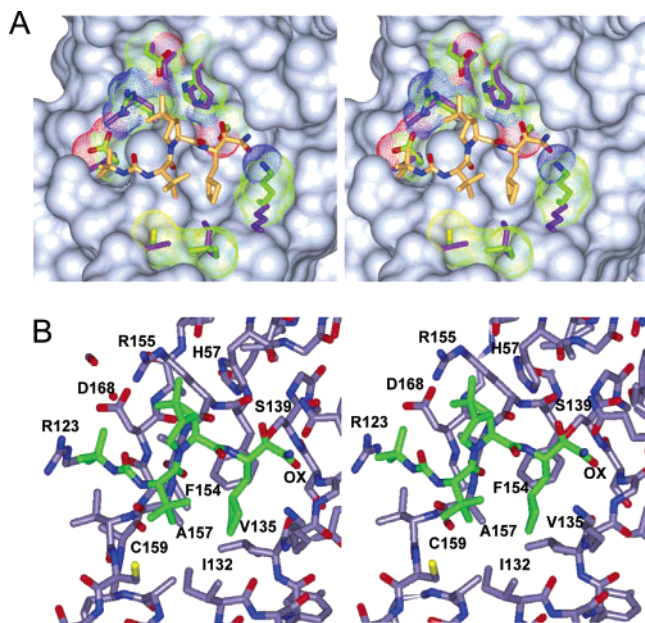


Figure 5. Protease–19 complex. Both panels are stereo representations. Panel A: The bulk of the protein is shown as a Connolly surface, while residues that undergo rotations upon forming a complex with the inhibitor are shown as sticks in atom specific coloring (green for carbon, red for oxygen, and blue for nitrogen) and dotted Connolly surfaces. The positions of the side chains in the holo-protease are shown as purple sticks. Panel B: Close-up of **19** in the binding site in stick form with colors: nitrogens (blue), oxygens (red), protein carbons (gray), and inhibitor carbons (green). Key residues forming the pockets are labeled with the single letter amino acid codes and their numbers. The oxyanion hole is labeled as OX.

Table 5. Average Torsions for Variable Side-Chain Conformations Observed in the Crystal Structures of 21 Protease–Inhibitor Complexes^a

side chain	conf.	# crystal structures examined	Chi1	Chi2	Chi3	Chi4
Arg123	holo		186	177	-75	-146
	A	9	187	175	-70	-157
	B	4	-69	-69	-167	78
Ile132	holo		-189	60		
	A	10	-169	58		
	B	4	-149	-74		
Lys136	holo		-182	-164		
	A	3	-147	151	58	60
	B	5	-170	-162	-188	165
Arg155	holo		-182	61	-173	180
	A	7	-72	-169	-179	155
	B		-173	-177	63	75
Cys159	holo		-177	-171	177	-97
	A	17	31			
Asp168	holo		58			
	A	19	-71	140		
	B	13	-175	85		
		8	-79	156		

^a Ile132: Chi1 = NCaCbCg1, Chi2 = CaCbCg1Cd1. Asp132: Chi2 = CaCbCgOd2.

S3 pocket. Arg123 and Asp168 have correlated conformational changes in the complexes to form either a bidentate salt bridge as in the holo-enzyme or a monodentate salt bridge. Ile132 has one dominant value of χ_1 (approximately -170) but assumes all three staggered χ_2 values. The conformation of Lys136 is highly variable and its side-chain atoms have high B-values.

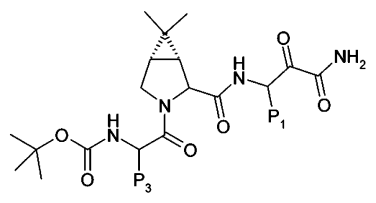
In the SBD of potent tripeptide inhibitors, P1 and P2 were found to give the biggest incremental increases in potency. Experimental inhibition constants are given for various P1 residues in Table 6. For acyclic residues (inhibitors **2–10**), Nva gives the most potent inhibitor. Examination of crystal structures

Table 6. P1 Structure–Activity Relationship

cmpd	P1	P3	X	K_i^*
2	Abu	Chg	O	740
3	Nva	Chg	N	54
4	Nva	Chg	O	100
5	Nva	<i>t</i> -Bug	O	220
6	Nle	<i>t</i> -Bug	O	360
7	Leu	Chg	O	400
8	Leu	<i>t</i> -Bug	O	480
9	<i>t</i> -Bua	<i>t</i> -Bug	O	> 3300
10	<i>t</i> -Bug	<i>t</i> -Bug	O	> 69 000
11	<i>c</i> -Prg	<i>t</i> -Bug	N	1600
12	<i>c</i> -Bug	<i>t</i> -Bug	N	100
13	<i>c</i> -Peg	<i>t</i> -Bug	N	1800
14	<i>c</i> -Pra	Chg	O	25
15	<i>c</i> -Bua	Chg	O	25
16	<i>c</i> -Pea	Chg	O	150
17	Cha	Chg	O	> 12 000
18	<i>c</i> -Pra	<i>t</i> -Bug	N	13
19	<i>c</i> -Bua	<i>t</i> -Bug	N	14
20	<i>c</i> -Pra-F ₂	<i>t</i> -Bug	N	50
21	<i>c</i> -Bua-F ₂	<i>t</i> -Bug	N	115
22	<i>c</i> -Pra	<i>t</i> -Bug	O	57

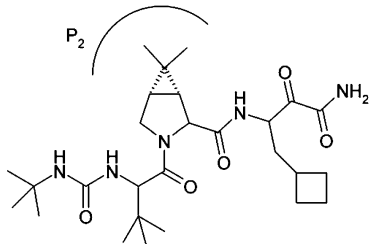
shows that Abu is too short to fill the S1 pocket, Nva fills the pocket more completely and Nle fills the pocket completely but causes some steric and torsional strain. Leu with γ -branching has about the same activity as Nle, but additional branching in *t*-Bua or *t*-Bug gives compounds with no measurable inhibition. Including both the cyclic and the acyclic residues, *c*-Pra and *c*-Bua are optimal. Cyclization removes the torsional penalty for binding eclipsed conformations of the side chains. *c*-Bua completely fills S1. In the protease–**14** complex, Ile132 and Lys136 adjust to make the pocket smaller so that *c*-Pra also completely fills S1. The slight size increase upon changing the distal CH₂ to CF₂ gives a significant loss in potency for both of these cyclic side chains (Compare **18/20** and **19/21** pairs in Table 6). For a subset of these inhibitors, which are defined by the generic formula *t*-Boc-Cha-(dimethyl-cyclopropyl)Pro-P1-CONH₂ and span a 30-fold range in potency, the relationship between inhibitor potency and surface area buried by P1 was examined. Because the structure of the S1 pocket varies somewhat even with the same P1, averages were computed for each P1, using 4–7 crystal structures related to the generic formula. Lacking a crystal structure with an Abu side chain at P1, the buried surface area was estimated by removing the terminal methyl group from Nva. Using this modeled Abu inhibitor as a reference, the relative experimental K_i^* values were predicted by the differential buried surface area within a factor of 0.3–1.1 for Nva, *c*-Pra, and *c*-Bua (Table 7) but 0.1 for Nle, a 10-fold discrepancy. Nle buries as much surface area as *c*-Bua but has introduced significant strain energy in both its conformation and that of S1, counteracting the favorable hydrophobic binding energy.

S2 is a partially closed cavity bounded on two sides by the faces of His57 and Arg155, while the Ala156 methyl group provides a small knob on a third side. The cavity is open toward the inhibitor backbone. His57 and Arg155 make polar interactions within or parallel to the cavity walls; these side chains do not project potential H-bonding groups into the cavity. This small cavity is filled by the C β and C δ atoms of P2 leucine in

Table 7. P1 Buried Surface Area—Activity Relationship


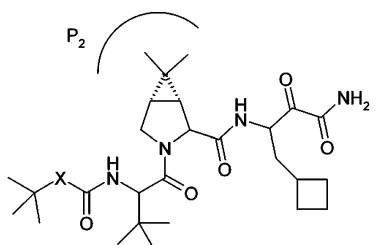
compd #	P1	P3	K_i^*	total SA	Δ SA	K_i^* SA, rel	K_i^* exp, rel	K_i^* exp/SA
2	Abu	Chg	740	82	0	1	1	1
4	Nva	Chg	100	120	38	18	7	0.4
22 ^a	Nle	Chg	160	136	54	63	5	0.1
14	c-Pra	Chg	25	125	43	27	30	1.1
15	c-Bua	Chg	25	141	59	93	30	0.3
5	Nva	<i>t</i> -Bug	220					
6	Nle	<i>t</i> -Bug	360					

^a Inhibitor **22** was not synthesized. Its K_i^* was estimated from that of **6** and the 2.2-fold decrease in K_i^* for Chg relative to *t*-Bug (ratio of K_i^* s for **5/4**).

Table 8. P2 Structure—Activity Relationship


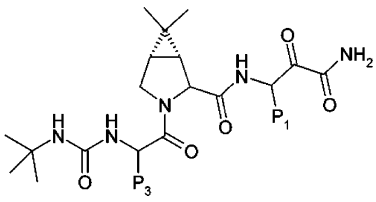
compd	P2	K_i^*
19	DMCP	14
23	DCCP	19
24	DFCP	140
25	DMFP	500
26	Pro	5000
37	ODBP	960

1 (Figure 2). P2 proline rigidifies the backbone in the bound conformation, but lacks the C δ contacts of leucine and loses about 5-fold in potency. Lacking analogs for direct comparison, this conclusion is based on affinity ratios for Leu/DMCP (compds **28/5**) versus Pro/DMCP (compds **26/19**). Proline was used as a scaffold for rigid leucine analogs culminating in **19** with dimethylcyclopropylproline (DMCP; Table 8). The rigid DMCP fills S2 better than leucine and gives a substantial increase in potency (70-fold relative to Leu, 350-fold relative to Pro). Replacing the two distal methyl groups with isosteric chlorines gives an inhibitor with equal potency. The difluoro analog is too small to completely fill S2 and loses potency. The dimethylfuranlyproline (DMFP, **25**) and the 1-oxo-2-dimethylcyclobutylproline analogs (ODBP, **35**, **36**) will be discussed below. Inhibitor potency versus surface area buried by P2 was examined for inhibitors that span a 90-fold potency range and have the generic formula *t*-Bu-urea-Bug-P2-*c*-Bua-CONH₂. Comparison of multiple crystal structures with the same P2 showed little variation in S2. The reference surface area for a Pro as residue P2 was calculated as an average of two crystal structures, but all other values were calculated from a single-crystal structure related to the generic formula for each P2. The relative potency of the cyclopropyl-Pro inhibitors is underestimated by a factor of 4–8 by the buried surface area (Table 9). By contrast, the relative potencies of the Leu, DMFP, and ODBP are overestimated by a factor of 3–20. For Leu, the lower potency is thought to arise from its greater backbone and side-

Table 9. P2 Buried Surface Area—Activity Relationship


compd	P2	X	K_i^*	total buried	Δ from Pro	K_i^* SA	rel K_i^* exp	rel K_i^* exp/SA
26	Pro	NH	5000	25 ^a	0	1	1	1
27 ^b	Leu	NH	1000	63	38	19	5	0.3
19	DMCP	NH	14	83	58	86	360	4.1
23	DCCP	NH	19	70	45	32	260	8.1
24	DFCP	NH	140	51	26	7	36	4.8
25	DMFP	NH	500	78	53	60	10	0.2
37	ODBP	NH	960	85	60	100	5	0.05
5	DMCP	O	220					
28	Leu	O	15 000					

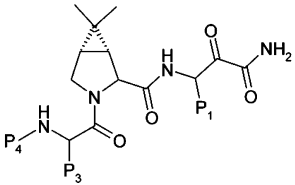
^a Average from two structures. ^b Inhibitor **27** was not synthesized. Its K_i^* was estimated from that of **28** and the 16-fold decrease in K_i^* for *t*-butyl urea relative to *t*-Boc (ratio of K_i^* s for **5/19**).

Table 10. P3 Buried Surface Area—Activity Relationship


compd	P1	P3	K_i^*	buried SA	Δ SA vs Val	K_i^* SA, rel	K_i^* exp, rel	K_i^* exp/SA
29	<i>c</i> -Pra	Val	100	37	0	1.0	1	1.0
30	<i>c</i> -Pra	Chg	50	55	18	4.0	2	0.5
19	<i>c</i> -Bua	<i>t</i> -Bug	14	34	-3	0.8	7	9.0
18	<i>c</i> -Pra	<i>t</i> -Bug	13	34	-3	0.8	8	9.7

chain flexibility. DMFP and ODBP have comparable rigidity to the cyclopropylproline-containing inhibitors DMCP and DCCP and bury comparable amounts of nonpolar surface. Compared to DMCP, the two methyl groups are shifted by 0.5 and 1.3 Å in ODBP and 0.8 and 1.8 Å in DMFP. For ODBP versus DMCP, the proline ring atoms C γ , C δ , and N shift by 0.5, 0.8, and 0.3 Å, respectively. Perhaps these shifts weaken binding interactions or are indicative of bicyclic ring strain in the bound conformation, but the reasons for the lower potency of DMFP and ODBP are difficult to pinpoint via molecular mechanics calculations or geometric considerations.

S3 is a small depression bounded by Ile132, Ala157, and Cys159. For the three P3 groups considered, the experimental potency varies only 8-fold (Table 10). Correlations between buried surface area and potency were examined for inhibitors of the generic formula *t*-Bu-urea-P3-DMCP-P1-CONH₂, with P1 = *c*-Pra or *c*-Bua (generally these two P1s give equipotent inhibitors). Because S3 is somewhat variable, buried surface areas were calculated as averages of two to three structures. Val binds with the two methyls of its isopropyl group forming a "V" pointing away from the surface and the hydrogen pointed down (Figure 2B). Together these two methyls bury about as much surface area as a single fully buried methyl (30 Å²; Table 10).²⁸ Chg buries more surface area, leading to a prediction of

Table 11. P4 Buried Surface Area–Activity Relationship


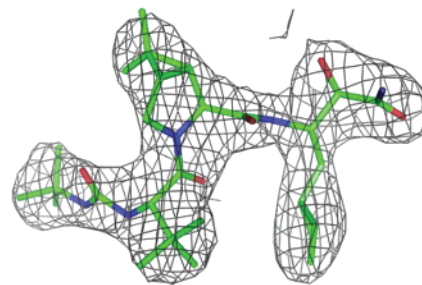
cmpd	P1	P3	P4	K_i^*	buried SA	K_i^* SA, rel	K_i^* exp, rel	K_i^* exp/SA
31^a	<i>c</i> -Pra	Chg	MeO(CO)	800	0 ^b	1	1	1
32^a	<i>c</i> -Pra	Chg	EtO(CO)	230	22	5	3	0.6
33^a	<i>c</i> -Pra	Chg	<i>i</i> -PrO(CO)	60	52	54	13	0.2
14	<i>c</i> -Pra	Chg	<i>t</i> -BuO(CO)	25	52	54	32	0.6
34^c	<i>c</i> -Pra	Chg	Ac-Val	68	55	68	12	0.2
35	<i>c</i> -Bua	<i>t</i> -Bug	Ac-Val	38				
19	<i>c</i> -Bua	<i>t</i> -Bug	<i>t</i> -BuNH(CO)	14				

^a Surface area based on X-ray structure of protease/**14** with various P4s modeled by removing carbons from the *t*-Boc group. ^b Buried surface area of the methyl group is zero so that the total buried surface area for the other groups is also the change from P4 of **31**. ^c Inhibitor **34** not synthesized. Its K_i^* was estimated from that of **35** using the ratio of K_i^* of **14/19** to correct for the change of P1 from *c*-Bua to *c*-Pra and P3 from *t*-Bug to Chg.

a modest potency increase as observed experimentally. *t*-Bug buries about the same surface area as Val, but largely by means of the third methyl group that points directly toward the enzyme surface (Figure 5). The 8-fold increase in potency of *t*-Bug over Val inhibitors is under predicted by a factor of 10 from the buried surface area. When *t*-Bug is compared to Chg, its smaller buried surface area should give 5-fold less potency, but it is 4-fold more potent with the *t*-butyl-urea cap (Table 10) and 2-fold less potent with the *t*-Boc cap (Table 7). These potency differences are comparable to the experimental error of 2–3-fold. The greater than expected activity of the *t*-Bug-containing inhibitors is probably due to greater rigidity and decreased entropic penalty for binding, which are apparently more important factors than buried surface area in the optimization of the P3 side chain.

The *t*-butyl-urea cap of **19** occupies S4. It affords about a 3-fold increase in potency over a conventional P4, such as *N*-acetyl-Val in **35**, while reducing the molecular weight and the number of amide bonds. Both urea NHs H-bond to Ala157 CO, and this gives a 2-fold increase in potency compared to *t*-Boc. In the series Cap-Chg-DMCP-*c*-Pra-CONH₂, where Cap = ROCO, the progressive 30-fold increase in potency for R = Me, Et, *i*-Pr, and *t*-Bu is well predicted by the increased buried surface area, which was modeled based on the structure of the Cap = *t*-Boc inhibitors (Table 11). Although Ac-Val buries slightly more surface area, it gives a less potent inhibitor than *t*-Boc. Boc binds in a somewhat different location than Val, shifted toward the top of the binding pocket and also would have a lower entropic penalty for binding.

The optimized tripeptide inhibitor **19**, *t*-Bu-urea-*t*-Bug-DMCP-*c*-Bua-CONH₂, is highly potent, with a K_i^* of 14 nM. The structure of its complex with protease (Figure 5) shows each residue interacting with its binding subsite. Notable elements are *c*-Bua, filling the S1 cavity, and DMCP, binding to the S2 surface as well as buttressing the catalytic triad in its active conformation. Rearrangements of the protease side chains from the holo-form to the inhibitor complex are shown (Figure 5A) as well as all of the side chains in the binding pocket (Figure 5B). Features that contribute to binding include the formation of a reversible covalent bond, hydrogen bonds, and the hydrophobic effect of burying nonpolar surface area. Nonpolar side

**Figure 6.** 2Fo–Fc electron density around inhibitor **19** is presented. This figure was generated using the program Pymol.³⁵

chains were varied systematically in the discovery process, culminating in the burial of 310 Å² of combined inhibitor and enzyme surface area, with about half from each source in the protease–**19** complex (Figure 6). *c*-Bua at P1 is 80% buried and contributes the largest factor to binding, followed by P2, P3, and P3-cap. The latter three groups are only ~40% buried, which highlights the exposed nature of this protease binding site.

Discussion

Crystallographic structures of protease–inhibitor complexes provided a basis for interpreting each inhibitor's potency relative to its complementarity to the protease binding site. Optimizing the fit of P1 and P2 to their subsites was especially important. The open nature of the protease binding site limited the noncovalent affinity that could be obtained. This lower affinity was compensated by forming a covalent adduct between the keto amide of the inhibitors and the active site serine. The optimized tripeptide was substantially lower in molecular weight than the original undecapeptide lead inhibitors. The physical and pharmacological properties of **19** were also optimized.²³ This compound has successfully completed phase I clinical studies and has advanced to phase II as a potential treatment for hepatitis C infections.²⁵

References

- (1) Consensus Panel. EASL International Consensus Conference on Hepatitis C, Paris, 26–28 February 1999, Consensus Statement. *J. Hepatol.* **1999**, *30*, 956.
- (2) (a) McHutchison, J. G.; Gordon, S. C.; Schiff, E. R.; Shiffman, M. L.; Lee, W. M.; Rustgi, V. K.; Goodman, Z. D.; Ling, M.-H.; Cort, S.; Albrecht, J. K. Interferon alpha-2b alone or in combination with ribavirin as initial treatment for chronic hepatitis C. *N. Engl. J. Med.* **1998**, *339*, 1485–1492. (b) Davis, G. L.; Estaban-Mur, R.; Rustgi, V.; Hoefs, J.; Gordon, S. C.; Trepo, C.; Schiffman, M. L.; Zeuzem, S.; Craxi, A.; Ling, M.-H.; Albrecht, J. Interferon alpha-2b alone or in combination with ribavirin for treatment of relapse of chronic hepatitis C. *N. Engl. J. Med.* **1998**, *339*, 1493–1499. (c) Zeuzem, S.; Feinman, S. V.; Rasenack, J.; Heathcote, E. J.; Lai, M.-Y.; Gane, E.; O'Grady, J.; Reichen, J.; Diago, M.; Lin, A.; Hoffman, J.; Brunda, M. J.; Peg-interferon alpha-2a in patients with chronic hepatitis C. *N. Engl. J. Med.* **2000**, *343*, 1666–1672. (d) Heathcote, E. J.; Schiffman, M. L.; Cooksley, W. G. E.; Dusheiko, G. M.; Lee, S. S.; Balart, L.; Reindollar, R.; Reddy, R. K.; Wright, T. L.; Lin, A.; Hoffman, J.; DePamphilis, J. Peg-interferon alpha-2a in patients with chronic hepatitis C and cirrhosis. *N. Engl. J. Med.* **2000**, *343*, 1673–1680.
- (3) De Francesco, R.; Tomei, L.; Altamura, S.; Summa, V.; Migliaccio, G. Approaching a new era for hepatitis C therapy: Inhibitors of the NS3–4a serine protease and the NS5b RNA-dependent RNA polymerase. *Antiviral Res.* **2003**, *58*, 1–16.
- (4) Kim, J. L.; Morgenstern, K. A.; Lin, C.; Fox, T.; Dwyer, M. D.; Landro, J. A.; Chambers, S. P.; Markland, W.; Lepre, C. A.; O'Malley, E. T.; Harbeson, S. L.; Rice, C. M.; Murcko, M. A.; Caron, P. R.; Thomson, J. A. Crystal structure of the hepatitis C virus NS3 protease domain complexed with a synthetic NS4A cofactor peptide. *Cell* **1996**, *87*, 343–355.
- (5) Love, R. A.; Parge, H. E.; Wickersham, J. A.; Hostomsky, Z.; Habuka, N.; Moomaw, E. W.; Adachi, T.; Hostomska, Z. The crystal structure of hepatitis C virus NS3 proteinase reveals a trypsin-like fold and a structural zinc binding site. *Cell* **1996**, *87*, 331–342.

- (6) Barbato, G.; Cicero, D. O.; Nardi, M. C.; Steinkühler, C.; Cortese, R.; De Francesco, R.; Bazzo, R. The solution structure of the N-terminal proteinase domain of the hepatitis C virus (HCV) NS3 protein provides new insights into its activation and catalytic mechanism. *J. Mol. Biol.* **1999**, *289*, 371–384.
- (7) Yao, N.; Reichert, P.; Taremi, S. S.; Prosis, W. W.; Weber, P. C. Molecular views of viral polyprotein processing revealed by the crystal structure of the hepatitis C virus bifunctional protease-helicase. *Structure (London)* **1999**, *7*, 1353–1363.
- (8) Gallinari, P.; Brennan, D.; Nardi, C.; Brunetti, M.; Tomei, L.; Steinkühler, C.; De Francesco, R. Multiple enzymatic activities associated with recombinant NS3 protein of hepatitis C virus. *J. Virol.* **1998**, *72*, 6758–6769.
- (9) Ingallinella, P.; Altamura, S.; Bianchi, E.; Taliani, M.; Ingenito, R.; Cortese, R.; De Francesco, R.; Steinkühler, C.; Pessi, A. Potent peptide inhibitors of human hepatitis C virus NS3 protease are obtained by optimizing the cleavage products. *Biochemistry* **1998**, *37*, 8906–8914.
- (10) Cicero, D. O.; Barbato, G.; Koch, U.; Ingallinella, P.; Bianchi, E.; Nardi, M. C.; Steinkühler, C.; Cortese, R.; Matassa, V.; De Francesco, R.; Pessi, A.; Bazzo, R. Structural characterization of the interactions of optimized product inhibitors with the N-terminal proteinase domain of the hepatitis C virus (HCV) NS3 protein by NMR and modelling studies. *J. Mol. Biol.* **1999**, *289*, 385–396.
- (11) Llinas-Brunet, M.; Bailey, M. D.; Bolger, G.; Brochu, C.; Faucher, A.-M.; Ferland, J. M.; Garneau, M.; Ghio, E.; Gorys, V.; Grand-Maitre, C.; Halmos, T.; Lapeyre-Paquette, N.; Liard, F.; Poirier, M.; Rheume, M.; Tsantrizos, Y. S.; Lamarre, D.; Structure-activity study on a novel series of macrocyclic inhibitors of the hepatitis C virus NS3 protease leading to the discovery of BILN 2061. *J. Med. Chem.* **2004**, *47*, 1605–1608.
- (12) Lamarre, D.; Anderson, P. C.; Bailey, M.; Beaulieu, P.; Bolger, G.; Bonneau, P.; Bös, M.; Cameron, D. R.; Cartier, M.; Cordingley, M. G.; Faucher, A.-M.; Goudreau, N.; Kawai, S. H.; Kukolj, G.; Lagacé, L.; LaPlante, S. R.; Narjes, H.; Poupart, M.-A.; Rancourt, J.; Sentjens, R. E.; George, T. S.; Simoneau, B.; Steinmann, G.; Thibeault, D.; Tsantrizos, Y. S.; Weldon, S. M.; Yong, C.-L.; Llinas-Brunet, M. An NS3 protease inhibitor with antiviral effects in humans infected with hepatitis C virus. *Nature* **2003**, 186–189.
- (13) Tsantrizos, Y. S.; Bolger, G.; Bonneau, P.; Cameron, D. R.; Goudreau, N.; Kukolj, G.; LaPlante, S. R.; Llinas-Brunet, M.; Nar, H.; Lamarre, D. Macrocyclic inhibitors of the NS3 protease as potential therapeutic agents of hepatitis C virus infection. *Angew. Chem., Int. Ed.* **2003**, *42*, 1356–1360.
- (14) Goudreau, N.; Cameron, D. R.; Bonneau, P.; Gorys, V.; Plouffe, C.; Poirier, M.; Lamarre, D.; Llinas-Brunet, M. NMR structural characterization of peptide inhibitors bound to the hepatitis C virus NS3 protease: Design of a new P2 substituent. *J. Med. Chem.* **2004**, *47*, 123–132.
- (15) Perni, R. B.; Pitlik, J.; Britt, S. D.; Court, J. J.; Courtney, L. F.; Deininger, D. D.; Farmer, J. L.; Gates, C. A.; Harbeson, S. L.; Levin, R. B.; Lin, C.; Lin, K.; Moon, Y.-C.; Luong, Y.-P.; O'Malley, E. T.; Rao, B. G.; Thomson, J. A.; Tung, R. D.; Van Drie, J. H.; Wei, Y. Inhibitors of hepatitis C virus NS3-4A protease 2. Warhead SAR and optimization. *Bioorg. Med. Chem. Lett.* **2004**, *14*, 1441–1446.
- (16) Perni, R. B.; Farmer, J. L.; Cottrell, K. M.; Court, J. J.; Courtney, L. F.; Deininger, D. D.; Gates, C. A.; Harbeson, S. L.; Kim, J. L.; Lin, C.; Lin, K.; Luong, Y.-P.; Maxwell, J. P.; Murcko, M. M.; Pitlik, J.; Rao, B. G.; Schairer, W. C.; Tung, R. D.; Van Drie, J. H.; Wilson, K.; Thomson, J. A. Inhibitors of hepatitis C virus NS3-4A protease. Part 3: P2 proline variants. *Bioorg. Med. Chem. Lett.* **2004**, *14*, 1939–1942.
- (17) Arasappan, A.; Njoroge, F. G.; Parekh, T. N.; Yang, X.; Pichardo, J.; Butkiewicz, N.; Prongay, A.; Yao, N.; Girijavallabhan, V. Novel 2-oxoimidazolidine-4-carboxylic acid derivatives as hepatitis C virus NS3-4A serine protease inhibitors: Synthesis, activity, and X-ray crystal structure of an enzyme inhibitor complex. *Bioorg. Med. Chem. Lett.* **2004**, *14*, 5751–5755.
- (18) Arasappan, A. A.; Njoroge, F. G.; Chan, T.-Y.; Bennett, F.; Bogen, S. L.; Chen, K.; Gu, H.; Hong, L.; Jao, E.; Liu, Y.-T.; Lovey, R. G.; Parekh, T.; Pike, R. E.; Pinto, P.; McKittrick, B.; Saksena, A. K.; Girijavallabhan, V.; Pichardo, J.; Butkiewicz, N.; Ingram, R.; Malcolm, B.; Prongay, A.; Yao, N.; Marten, B.; Madison, V.; Kemp, S.; Levy, O.; Lim-Wilby, M.; Tamura, S.; Ganguly, A. K. Hepatitis C virus NS3-4A serine protease inhibitors: SAR of P2 moiety with improved potency. *Bioorg. Med. Chem. Lett.* **2005**, *15*, 4180–4184.
- (19) Venkatraman, S.; Njoroge, F. G.; Girijavallabhan, V.; Madison, V.; Yao, N.; Prongay, A. J.; Butkiewicz, N.; Pichardo, J. Design and synthesis of depeptidized macrocyclic inhibitors of hepatitis C NS3-4A protease using structure-based drug design. *J. Med. Chem.* **2005**, *48*, 5088–5091.
- (20) Bogen, S.; Saksena, A. K.; Arasappan, A.; Gu, H.; Njoroge, F. G.; Girijavallabhan, V.; Pichardo, J.; Butkiewicz, N.; Prongay, A.; Madison, V. Hepatitis C virus NS3-4A serine protease inhibitors: Use of a P2–P1 cyclopropyl alanine combination for improved potency. *Bioorg. Med. Chem. Lett.* **2005**, *15*, 4515–4519.
- (21) Chen, K. X.; Njoroge, F. G.; Pichardo, J.; Prongay, A.; Butkiewicz, N.; Yao, N.; Madison, V.; Girijavallabhan, V. Design, synthesis, and biological activity of *m*-tyrosine-based 16- and 17-membered macrocyclic inhibitors of hepatitis C virus NS3 serine protease. *J. Med. Chem.* **2005**, *48*, 6229–6235.
- (22) Lin, C.; Lin, K.; Luong, Y. P.; Rao, B. G.; Wei, Y. Y.; Brennan, D. L.; Fulghum, J. R.; Hsiao, H. M.; Ma, S.; Maxwell, J. P.; Cottrell, K. M.; Perni, R. B.; Gates, C. A.; Kwong, A. D. In vitro resistance studies of hepatitis C virus serine protease inhibitors, VX-950 and BILN 2061: Structural analysis indicates different resistance mechanisms. *J. Biol. Chem.* **2004**, *279*, 17508–17514.
- (23) Venkatraman, S.; Bogen, S. L.; Arasappan, A.; Bennett, F.; Chen, K.; Jao, E.; Liu, Y.-T.; Lovey, R. G.; Hendrata, S.; Huang, Y.; Pan, W.; Parekh, T.; Pinto, P.; Popov, V.; Pike, R. E.; Ruan, S.; Santhanam, B.; Vibulbhan, B.; Wu, W.; Kong, J.; Liang, X.; Wong, J.; Liu, R.; Butkiewicz, N.; Chase, R.; Hart, A.; Agrawal, S.; Ingravallo, P.; Pichardo, J.; Guo, Z.; Prongay, A.; Broske, L.; Cui, X.; Cheng, K.-C.; Hsieh, T. Y.; Brisson, J.-M.; Prelusky, D.; Bogdanowich-Knipp, S.; Pavlovsky, A.; Saksena, A.; Girijavallabhan, V.; Njoroge, F. G.; Madison, V.; Baroudy, B.; Malcolm, B.; Korfmacher, W.; White, R.; Bradley, P. Discovery of (1*R*,5*S*)-*N*-[3-amino-1-(cyclobutylmethyl)-2,3-dioxopropyl]-3-[2(*S*)-[[[1,1-dimethylethylamino]carbonyl]amino]-3,3-dimethyl-1-oxobutyl]-6,6-dimethyl-3-azabicyclo[3.1.0]hexan-2(*S*)-carboxamide (Sch 503034), a selective, potent, orally bioavailable HCV NS3 protease inhibitor: A potential therapeutic agent for the treatment of hepatitis C infection. *J. Med. Chem.* **2006**, *49*, 6074–6086.
- (24) Perni, R. B.; Britt, S. D.; Court, J. C.; Courtney, L. F.; Deininger, D. D.; Farmer, L. J.; Gates, C. A.; Harbeson, S. L.; Kim, J. L.; Landro, J. A.; Levin, R. B.; Luong, Y.-P.; O'Malley, E. T.; Pitlik, J.; Rao, B. G.; Schairer, W. C.; Thomson, J. A.; Tung, R. D.; Van Drie, J. H.; Wei, Y. Inhibitors of hepatitis C virus NS3-4A protease 1. Non-charged tetrapeptide variants. *Bioorg. Med. Chem. Lett.* **2003**, *13*, 4059–4063.
- (25) Zeuzem, S.; Sarrazin, C.; Homburg, F.; Rouzier, R.; Forestier, N.; Gupta, S.; Hussain, M.; Shah, A.; Cutler, D. L.; Zhang, J. *Combination therapy with the HCV protease inhibitor, SCH 503034, plus PEG-intron in hepatitis C genotype-1 PEG-intron non-responders: Phase Ib results*; Proceedings of the American Association for the Study of Liver Diseases (AASLD), San Francisco, CA, November 11–15, 2005. Francisco, CA, 2005; Hepatology Abstract 67627.
- (26) Otwinowski, Z.; Minor, W. Processing of X-ray diffraction data collected in oscillation mode. In *Methods of Enzymology: Macromolecular Crystallography, part A*; Carter, C. W., Jr., Sweet, R. M., Eds.; Academic Press: New York, 1997; Vol. 276, pp 307–326.
- (27) Brünger, A. T. *X-PLOR, version 3.1 manual: a system for X-ray crystallography and NMR*; Yale University Press: New Haven, CT, 1993.
- (28) Tanford, C. The Hydrophobic Effect. *Formation of Micelles and Biological Membranes*, 2nd edition; John Wiley and Sons: New York, 1980.
- (29) Sybyl; Tripos Associates: St. Louis, MO.
- (30) Quantum Chemistry Program Exchange, program 429, Indiana University, Bloomington, Indiana.
- (31) Zhang, R.; Beyer, B. M.; Durkin, J.; Ingram, R.; Njoroge, F. G.; Windsor, W. T.; Malcolm, B. A. A continuous spectrophotometric assay for the hepatitis C virus serine protease. *Anal. Biochem.* **1999**, *270*, 268–275.
- (32) Morrison, J. F.; Walsh, C. T. *Adv. Enzymol.* **1988**, *61*, 201–301.
- (33) Kraulis, P. J. MOLSCRIPT: a program to produce both detailed and schematic plots of protein structures. *J. Appl. Crystallogr.* **1991**, *24*, 946–950.
- (34) *InsightIII*; Molecular Simulations Inc.: 9685 Scranton Road, San Diego, CA, 92121–3752
- (35) DeLano, W. L. *The Pymol Molecular Graphics System*; DeLano Scientific LLC: San Carlos, California, 2002.